THE ASTROPHYSICAL JOURNAL, 247:488–498, 1981 July 15

DENSITY-WAVE INDUCED STAR FORMATION: A MODEL FOR M81

FRANK N. BASH
Department of Astronomy, The University of Texas at Austin
AND
H. C. D. VISSER
Berkeley Astronomy Department
Received 1980 July 31; accepted 1981 February 4

ABSTRACT

The two-armed spiral shock (TASS) wave, fitted to observations of the H I gas in M81 by Visser, is used to give initial conditions for ballistic particles launched from the spiral arms. The model predicts the location of molecular clouds which agrees with the one detection of CO in M81. In addition, our model agrees with the observed distribution of H II regions near the eastern arm. The model also predicts the radial velocities of, and velocity differences between, H II regions and molecular clouds near the major and minor axes. When the model's disk linear density wave amplitude, spiral arm star mass function, and star formation rate are fitted to observations of the surface brightness, the predicted arm colors agree best with the observed ones when we use a linear density wave amplitude very near the observed one. The spiral arm stellar mass function required for this agreement suggests that spiral arms essentially make only O and B stars or that low-mass stars are hidden or not yet formed while the O and B stars are shining. The model also produces a galaxy which resembles a photograph of M81.

Limitations and consequences of this work are given, and suggestions are made for specific observational and theoretical projects.

Subject headings: galaxies: internal motions — galaxies: photometry — galaxies: structure — interstellar: molecules — stars: formation — stars: stellar dynamics

I. INTRODUCTION

This paper represents a preliminary study of M81 in which previously published models are applied to M81. We plan a larger study which will involve modifications of our published models and possibly new observations. The intention here is to solicit comment and specific observations with which we can check, and hopefully improve, our models.

Visser (1978) fitted the two-armed spiral shock (TASS) wave to H I observations of M81. Bash and Peters (1976, hereafter Paper I), Bash, Green, and Peters (1977, hereafter Paper II), and Bash (1979, hereafter Paper III) proposed a dynamical model suggesting a connection among a galaxy's spiral structure, dense molecular gas, and spiral arm star formation. In that series of papers a somewhat convoluted case was presented for a model which describes the dynamics of dense molecular clouds, originating in the density-wave spiral arms, which produce stars and the galaxy's optical spiral arms. The model predicted that giant molecular clouds would be found to be tightly confined to a region near the spiral arms. This prediction seems now to be most convincingly confirmed by Stark (1979), who surveyed the CO distribution along the minor axis of M31. The model also explains why the expected rapid rise and slow decay of optical surface brightness and color across spiral arms are seldom seen in spiral galaxies. The convolutions in the case supporting our model arise due to the great mixture of evidence required. The dynamical model required H I, 21 cm line data to fit the spiral pattern to the Galaxy, CO observations in the Galaxy to find the molecular clouds, optical and radio observations of open star clusters to confirm the limited lifetimes of molecular clouds, and a comparison of the dynamical model fit to the Galaxy and optical observations of other galaxies in order to deduce properties of the star formation process in spiral arms. For the first time, using the work of Visser (1978), it is possible to apply the dynamical model entirely self-consistently to observations of one spiral galaxy M81.

In Papers I, II, and III we assert that dense molecular clouds form in the spiral pattern at the postshock velocity, and that these clouds then move ballistically under the influence of the galaxy's axisymmetric potential, perturbed by the spiral arms. We find that the clouds radiate the ^{12}CO $J=1\rightarrow 0$ spectral line at 115 GHz for 40 million years and that stars are seen in the clouds 25 million years after the cloud's birth in the TASS wave. We do not claim that this is the only mechanism for star

formation in spiral galaxies. There may be at least one more mechanism, unconnected with the arms, which produces primarily low-mass stars. Also, in the spiral-arm star formation process, the density-wave mechanism may only act as the initiator for secondary processes in which one star causes the birth of others. These possibilities are discussed in Paper III. This paper deals only with one process, the density-wave (TASS wave) star formation process. In the arms it may be dominant in an early type, strong-armed galaxy like M81 (Roberts, Roberts, and Shu 1975). The dense molecular phase is largely undetected in M81. However, on the assumption that the dense clouds exist and make stars, the optical surface brightness and color predicted by the model can be compared with Schweizer's (1976) optical observations. Using Visser's (1978) model without *any* adjustment, we can integrate ballistic orbits beginning at the TASS wave with his postshock velocities used as initial values.

In § II we examine the position, distribution, and velocities of the ballistic particles in M81. The set of particles whose ages are no greater than 40 million years is expected to be the same as the distribution of dense molecular clouds (Paper III). We compare this predicted molecular cloud distribution with the one reported detection of CO in M81 (Combes *et al.* 1977). Since we infer that stars form in the dense clouds 25 million years after the cloud birth (Paper III), the distribution of particles whose ages are 25–40 million years might be expected to be similar to the distribution of massive stars and H II regions. We compare this distribution with the H II region distribution in M81 reported by Connolly, Mantarakis, and Thompson (1972) (CMT). Finally, although present observations are not sufficiently accurate to allow a comparison, we predict the velocities of, and velocity differences between, H II regions and CO clouds along the major and minor axes of M81.

In § III we compare predicted surface photometry against Schweizer's observations. His observations are used to adjust the linear density-wave amplitude in the old disk stars, the star formation rate in the spiral arms, and the stellar initial mass spectrum for our spiral arm process. We also attempt to account for reddening in the disk of M81. The model succeeds in producing a galaxy which resembles M81. We report the model's total star formation rate, the radial dependence of the star formation rate, and the radial run of spiral arm colors. Problems encountered in this comparison and suggestions for future work are also discussed. In most ways, M81 appears to be an ideal candidate for a definitive and detailed test of the importance of the density wave in determining the optical appearance of spiral galaxies.

II. THE DYNAMICAL MODEL

The galaxy M81 (NGC 3031) is classified as SA(s)ab in the Second Reference Catalogue (de Vaucouleurs, de Vaucouleurs, and Corwin 1976) and has been assigned to luminosity class I–II by van den Bergh (1960). In order to be consistent with Visser (1978), we adopt his values: an inclination angle of 59° to the plane of the sky, a position angle of 149° for the major axis, and a distance of 3.25 Mpc, although Ford and Jenner (1978) suggest a smaller distance. In addition we adopt, without change, Visser's values of the forcing function (the ratio of the spiral potential to the axisymmetric potential), the spiral potential minimum's inclination angle, its dependence on distance from the center of the galaxy, and his adopted rotation curve. As with Visser, the spiral potential minimum was forced to cross the major axis at 5.04 kpc from the center. The postshock velocities, computed by Visser for M81, are shown in Figure 1. The spiral inclination angles and the rotation curve were used to compute the velocities in a system perpendicular to V_R and tangent to $(V_c - V_\theta)$ circles centered on the galactic center. A velocity dispersion was introduced into the initial velocities by varying the value of $(V_c - V_\theta)$ by ± 5 km s^{-1}. All the postshock velocities are directed toward the galactic center and are slower than the circular velocity. The position of the TASS wave, with respect to the potential minimum, was taken from Figure 6.6 in Visser (1978).

Selected ballistic particle orbits are shown in Figure 2. The orbit of each particle was integrated for 100 million years. In Figure 2 the coordinate grid is centered on the center of M81 and it lies in the plane of the sky. The distance between tick marks is 1 kpc. The coordinate system in the plane of the galaxy is rotating at $\Omega_p = 18$ km s^{-1} kpc^{-1} in order to keep the spiral pattern fixed with respect to the grid. The horizontal axis in Figure 2

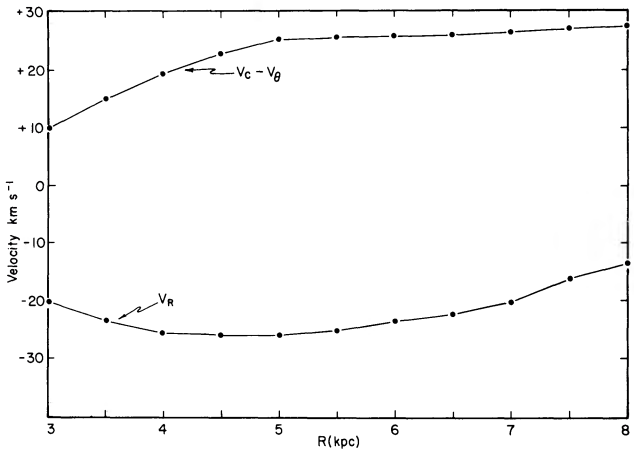

FIG. 1.—The initial velocities for the ballistic particles in our model. The radial component V_R is positive away from the center, and the tangential component V_θ is shown subtracted from the circular velocity V_C. Note that the radial component is directed toward the center and the tangential component is slower than the circular velocity. The tangential component was perturbed by ± 5 km s^{-1} to introduce a dispersion. These velocities are the postshock velocities computed by Visser (1978).

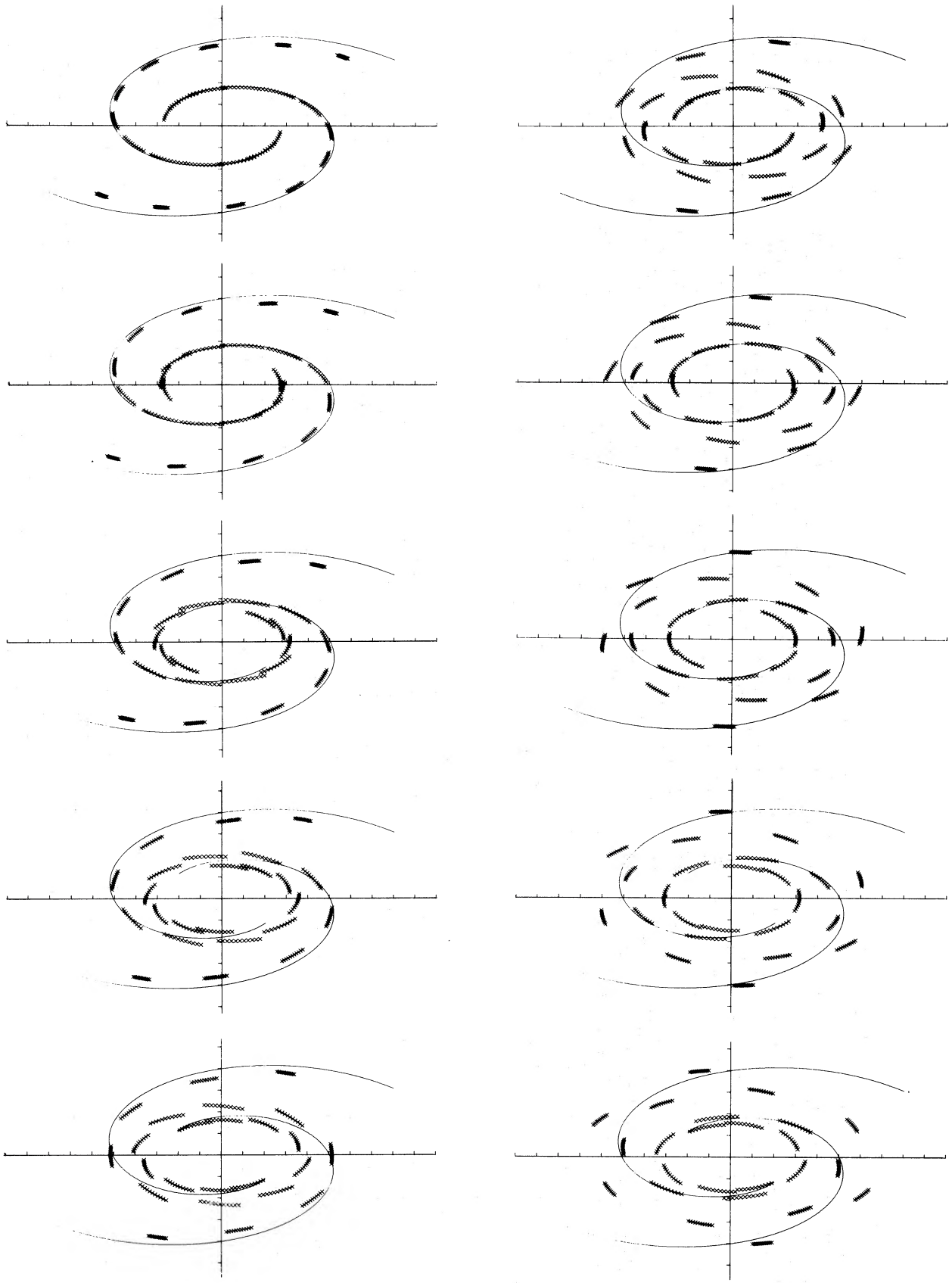

FIG. 2

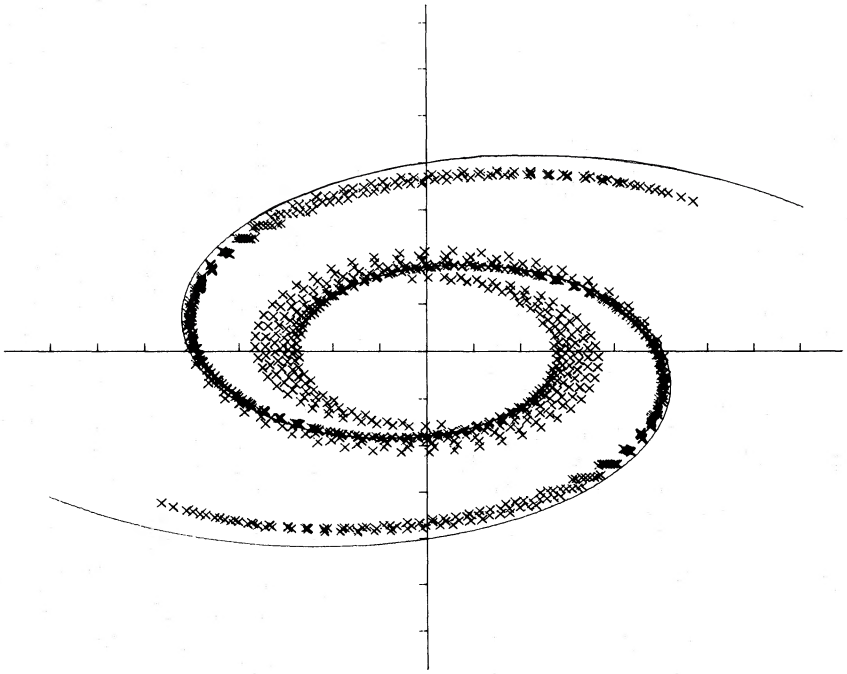

FIG. 3.—The instantaneous location of all ballistic particles having ages from zero through 40 million years in an inclined view, which should correspond with the location of molecular clouds. CO has been detected near the major axis (the abscissa), 3.4 kpc from the center using an antenna having a beamwidth of ~1 kpc at M81. The coordinate tick-marks are spaced by 1 kpc in the plane of the sky.

is the major axis, the particles move counterclockwise, and the spiral potential minimum (not the TASS wave) is drawn.

In Figure 2, particles begin their orbits at the TASS wave which lies inside the potential minimum. The length of each orbital path covers the same amount of time (100 million years). Note the particles launched at larger distances from the center of M81 tend to move along the inside of the spiral with most of their orbital track inside of the spiral. The particles launched closer to the center cross the spiral more quickly, spending a smaller fraction of their 100 million year track inside the potential minimum. This can be understood since particles in the outer regions start their orbit further from the potential minimum; also the relative velocity with respect to the spiral pattern is smaller.

Figure 3 shows the instantaneous areal distribution of ballistic particles having ages from 0 through 40 million years over the face of M81. This distribution depends on the dynamical model which we have discussed and on the radial birthrate for the ballistic particles. Together they control the surface density of particles at a given position, whereas the dynamical model alone controls the size, shape, and positions of the patches of particles in the model galaxy. The radial birthrate is discussed in the next section. It is a free parameter which has been adjusted so that the computed surface brightness in the optical U and B_3 bands agrees with observations made between 3.85 kpc and 7.48 kpc from the center of M81.

We now liken the ballistic particles in the model to dense molecular clouds which form stars. In Paper III, we claim that the dense molecular phase corresponds to the first 40 million years of the ballistic orbit and that stars are seen in the dense clouds 25 million years after the cloud's birth. Therefore we predicted an overlap of 15 million years in which one sees young stars and dense molecular gas together. Therefore Figure 3 represents our model's prediction for the location of the dense molecular gas in M81. Only one detection of the dense molecular gas in M81 has been reported. Combes *et al.* (1977) report the detection of CO in M81 using the NRAO Kitt Peak antenna which has a beamwidth of 1′. CO was detected near the major axis, 3.4 kpc southeast of the center of M81. This detection corresponds very

FIG. 2.—Selected particle orbits in a rotating frame, rotating at the pattern speed. The orbits are inclined to the sky by 59°. The major axis is the horizontal line, and the tick marks are spaced by 1 kpc on the plane of the sky. Each panel shows 10 million years of the orbit of selected particles, except for 11 million years in the upper-left panel. The position of each particle is marked by a cross each million years, and each panel shows different pieces of the same orbits. The upper-left panel shows particles from age zero through 10 million years. The bottom-left panel shows ages 41 through 50 million years, the top-right one shows ages 51 through 60 million years, and the bottom-right one shows ages 91 through 100 million years.

closely to the center of the wide region centered on the major axis at about 3.2 kpc from the center of M81 as shown in Figure 3. One might suppose that regions of angular size $\sim 1'$, in which the radial velocity spread is small, are favored for detection. At M81, $1' \approx 1$ kpc, so this region and the other one on the opposite side of the center are the only ones where a 1′ beam is filled by CO clouds. Although thin molecular arms are predicted to cross the major axis at about 5 kpc from the center, their angular width is only about 20″. In addition, Figure 5 shows that on the major axis, at $R \approx 3$ kpc, the CO is spread over a narrow range of radial velocity (~ 20 km s^{-1}) while the CO at $R \approx 5$ kpc is spread over ~ 70 km s^{-1}. This also causes the region near $R = 3$ kpc to be favored for detection. Combes *et al.* (1977) report searching several other positions in M81 for CO signals without detecting any. They do not report those positions. It is not clear why CO was not detected on the major axis 3.4 kpc northwest of the center; however, Rots and Shane (1975) and Rots (1975) point out that the H I gas is also asymmetrically distributed.

We can also compare predictions of the dynamical model to observations of the locations of H II regions in M81 made by CMT. We suppose that the first 15 million years after the stars turn on might correspond to the time during which H II regions form. In their Figure 3, CMT show a face-on plot of the H II regions in M81. In Figure 4 we show the face-on distribution of ballistic particles which, we claim, corresponds to the first 15 million years of the stars born from the spiral arms. This also corresponds to ballistic particle ages from 25 to 40 million years since we claim that star formation is preceded by a 25 million year gestation time in the molecular clouds. In Figure 4, the major axis runs horizontally. One first has to change the distance scale in CMT's Figure 3 since CMT's estimate of the distance to M81 (2.64 Mpc) is different from ours (3.25 Mpc). Also note that in their figure, north is at the bottom left. At first sight, there seems little detailed agreement between CMT's Figure 3 and our Figure 4. CMT's Figure 3 perhaps shows the thin spiral arm of young stars which our model predicts, lying from 3′ to 6′ to the right of and 1′ to 4′ above the center of M81 (the eastern arm) and a small bit of the corresponding arm the same distance below and to the left of the center (the western arm). The eastern arm is the one in which the best agreement between neutral hydrogen observations and the density wave model was found. In addition, the relatively empty areas beyond 4′ above and below the center perhaps correspond to the large empty regions predicted to lie between the thick inner arm and the thin outer arm above and below the model's center in Figure

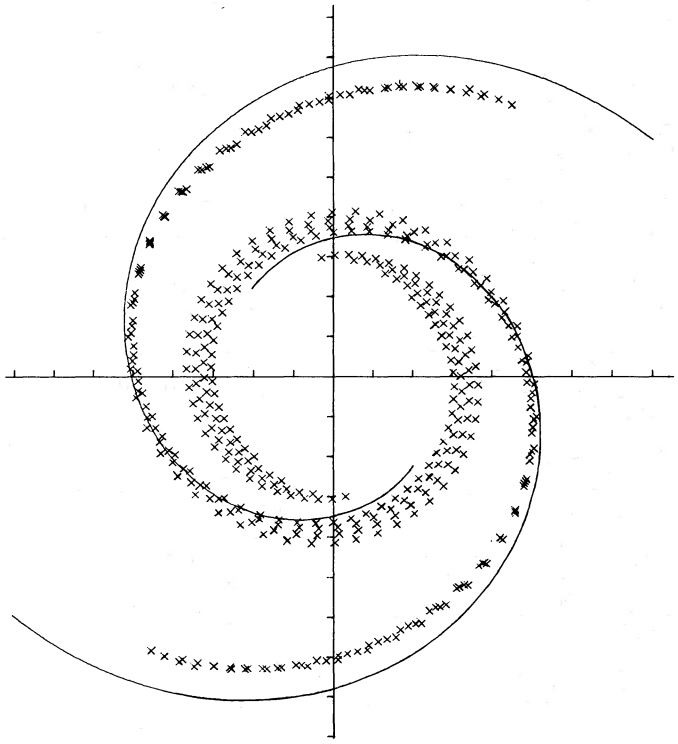

FIG. 4.—A face-on view with the same coordinate system, ticks spaced by 1 kpc in the plane of the galaxy and the potential minimum shown by the thin spiral. The crosses represent the location of the ballistic particles having ages from 25 through 40 million years which we claim corresponds to the distribution of H II regions.

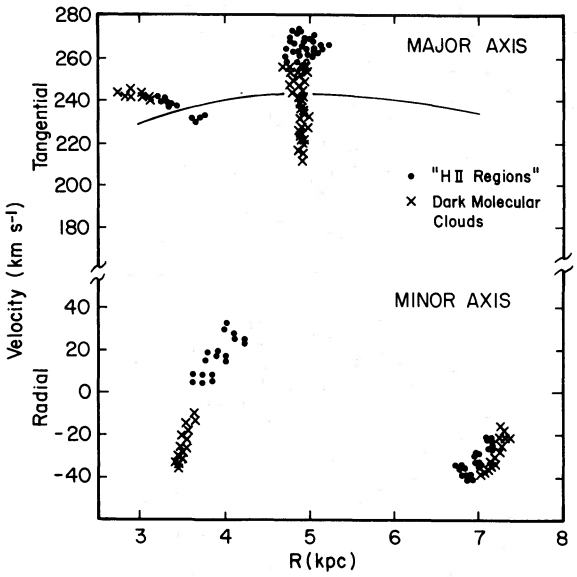

FIG. 5.—The predicted velocities of H II regions and dark molecular clouds. The former are ballistic particles of ages 26 through 40 million years while the latter are those particles ages zero through 25 million years. The velocities are expressed with respect to the center of, and in the plane of, M81. The radial component is positive away from the center of M81.

5. There are many H II regions shown in CMT's Figure 3 that are not predicted by the model, especially in the western part of the galaxy. Perhaps this is evidence that the "other" mechanism for star formation is dominant there. Mezger (1970) maintains that, in the Galaxy, only the giant H II regions reveal the spiral arms. Maybe the spiral structure could be more clearly seen in CMT's Figure 3 if the figure were to show only the giant H II regions rather than all of them.

Figure 5 shows predicted velocities for the ballistic particles shown in the previous two figures. At the top, Figure 5 shows predicted tangential velocities in the plane of M81 for ballistic particles less than 40 million years old and within 200 pc of the major axis. The velocities are with respect to the center of M81, expressed in the plane of the galaxy, and the rotation curve used in this study is shown. Particles of age no greater than 25 million years are plotted as crosses while those of $26 \leq \text{age} \leq 40$ million years are plotted as dots. At the bottom of Figure 5 we show the expected peculiar radial velocity for the particles within 200 pc of the minor axis again with respect to the center of and in the plane of M81, where positive velocities mean those directed away from the center of M81.

To clarify the convention, a velocity of 240 km s^{-1} on the major axis at $R=5$ kpc, as shown in Figure 5, would give an observed heliocentric radial velocity of 166 km s^{-1} for the northwest portion of the major axis taking into account the galaxy's inclination angle (59°), systemic velocity (-40 km s^{-1}), and sense of rotation (away from us on the northwest side). We expect that H II regions will be seen at the radial velocities shown by the dots while the crosses correspond to expected molecular cloud velocities for the clouds in which stars have not yet formed. A significant difference is predicted between the average molecular cloud and H II region velocity, along the major axis at $R \approx 5$ kpc and on the minor axis at $R \approx 3.8$ kpc, while very little difference is predicted on the major axis at $R \approx 3$ kpc and on the minor axis at $R \approx 7$ kpc. Future observations of these velocities will provide an important test of this model.

The velocity difference arises in our model since the "dark" and "H II region" phases represent different times in the evolution of a dense molecular cloud and different times along its ballistic orbit. This leads to a spatial separation of the two phases and a velocity difference for the two phases. But since the cloud orbits lie mostly along the spiral arms (see Fig. 2), the H II region phase of one cloud, coming from a certain birth site, spatially coincides with the dark phase of a different cloud which came from a downstream birth site. As can be seen on Figure 5, the radial separation of the centroids of the H II region arms and the dark molecular cloud arms is less than 500 pc in the best case. The current angular resolution of radio telescopes at the frequency of the $J=1 \rightarrow 0$ spectral line of CO is $\sim 1'$, which is ~ 1 kpc at M81. Radial velocity differences among spatially intermingled H II regions and dark clouds seem to be detectable predictions of the model.

The ballistic particle model, used here, is certainly not the only conceivable model for describing star formation in M81. That model is based on a physical plausibility —viz., that giant molecular clouds are sufficiently dense to behave ballistically over their lifetimes—and it seems to be consistent with observations as discussed here and in our previous papers. But an alternative model which might predict similar results is that the molecular gas moves along streamlines. We have computed the differences in position and velocity for a ballistic particle originating at the shock, on a streamline, at the post-shock velocity, and compared them with the position and velocity of the gas in the streamline for three different streamlines. Table 1 shows the results. The velocity and position differences at age zero are all zero. For each streamline whose mean radius is given, we tabulate the position difference between the streamline and the particle (Δd) in kpc and the tangential velocity difference (ΔV_θ) and radial velocity difference (ΔV_r), both in km s^{-1}. The position differences are not very large. They do not exceed 1 kpc until ages of 40 million years and beyond, but many velocity differences exceed 20 km s^{-1}. These velocity differences should be quite detectable. Specifically, we predict a velocity difference between H II regions (which we describe as ballistic particles) and H I gas (which should move on stream-

TABLE 1

POSITION AND VELOCITY DIFFERENCES BETWEEN BALLISTIC PARTICLES AND GAS STREAMLINES

	Streamline Mean Radius (kpc)								
	3.9			5.4			6.9		
Age (10^6 yr)	Δd (kpc)	ΔV_θ [a] (km s^{-1})	ΔV_r [a] (km s^{-1})	Δd (kpc)	ΔV_θ (km s^{-1})	ΔV_r (km s^{-1})	Δd (kpc)	ΔV_θ (km s^{-1})	ΔV_r (km s^{-1})
10.....	0.09	−5	−22	0.31	−9	−18	0.22	−9	−11
20.....	0.42	+8	−17	0.11	−3	−30	0.16	−7	−23
30.....	1.0	+12	+7	0.51	+10	−22	0.52	+1	−26
40.....	1.3	+5	+16	1.3	+18	0	1.3	+11	−17
50.....	1.2	−2	+27	1.9	+12	+12	2.2	+16	−1
60.....	1.0	+27 [b]	+21 [b]	2.3	+7	+9	3.1	+13	+10

[a] $\Delta V \equiv V$(particle) − V(streamline). V_θ is positive in the direction of rotation; V_r is positive outward from the center.
[b] The particle crosses the other arm between 50 and 60 million years.

lines) at the same location. Therefore we predict velocity differences among H I, H II regions and dark molecular clouds. Observations of these velocities are required in order to determine the correctness of the ballistic particle model.

III. *UBV* SURFACE BRIGHTNESS AND COLORS

We now ask the model to predict the distribution of light and color in M81. The dynamical model describes the trajectories of groups of stars born in dense clouds which have come off the arms at postshock velocities. We now associate each model ballistic particle with a star "cluster" and describe the cluster's mass spectrum by either model A, B, or C from Paper III. Model C is extremely rich in high-mass stars compared to model A, while B is an intermediate case.

The hydrodynamical model for the gas and the dynamical model for M81 control the location of the TASS wave with respect to the density-wave arms in the old disk, and thus they control the positions from which our model clouds are launched with respect to those red arms. In our model, the clouds move only under the influence of gravity and after 25 million years a group of stars is born in each cloud and the group ("cluster") continues along its galactic orbit. This delay, the location of the TASS wave, and our dynamical model control where this starlight will appear in the galaxy and where the young spiral arms will lie with respect to the broad, smooth arms of old, red stars. The mass spectrum of the young stars assumed to be born from the clouds determines the color and width of the arms of young stars. The reason the width is affected is that if only massive stars are born, the young stars will die relatively quickly and the arms will be narrower than arms of less massive stars. The mass spectrum of the young stars determines their luminosity per unit mass and together with the mass birthrate it controls the surface brightness of the spiral arms.

We use the M81 observations in Schweizer (1976). We adopt his values for the central surface brightness, color, and radial brightness gradient of the stellar disk which underlies the arms. We allow the disk to contain a linear density-wave whose amplitude we adjust, and we use Schweizer's values for the average surface brightness around circles of radii 3.86, 4.33, 4.81, 5.36, 5.99, 6.70 and 7.48 kpc. The model is forced to agree with Schweizer's values for the average surface brightness at the seven radii above and in both the U and B_3 bands. In order to reproduce both the observed average surface brightness and the spiral arm color, the model is severely constrained. The first condition controls the amount of light, from the linear density wave plus the new stars, which must be added to the smooth disk. The second condition controls the color of the light of the new stars which in turn is governed by their mass spectrum. A series of 10 models was constructed using different cluster mass spectra, different linear density-wave amplitudes, and different star formation rates. In each model except one, a star formation rate was found so that, on average, the model's surface brightness at the seven radii from $R=3.86$ to 7.48 kpc agreed with Schweizer's observations in both the U and B_3 bands to better than 0.1 mag arcsec^{-2}. The exception is the model using cluster model C and density wave amplitude 0.25 mag. In the B_3 band the difference was 0.12 mag arcsec^{-2}.

The amplitude of the linear density wave is a parameter which was set in Visser's model. There, it is called the "forcing" and is expressed as a percentage of the axisymmetric force. Our dynamical model uses the same forcing as Visser used. The free parameter discussed in the paragraph above is the surface brightness amplitude of the linear density wave. These two amplitudes will be equal only if the mass to light ratio of the old disk stars is constant around circles centered on the center of the galaxy, and the ratio of the two amplitudes will be constant all over the galaxy only if the mass to light

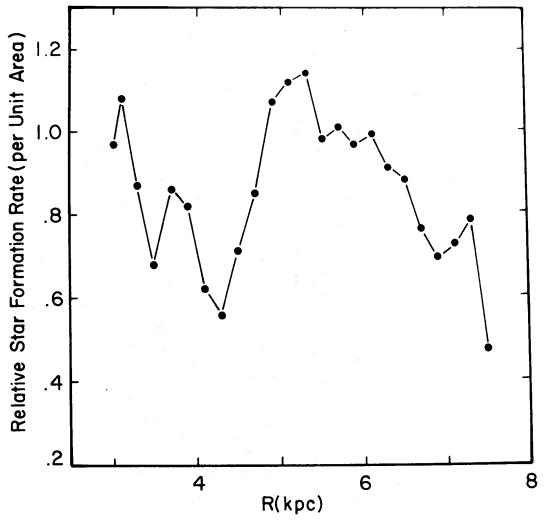

FIG. 6.—The relative, radial star-formation rate in M81 used for all the models plotted in Fig. 9. This rate allows the model to reproduce the observed surface brightness.

ratio of the old disk stars is constant. Therefore the surface brightness amplitude can be determined as a free parameter without contradicting the determination of the forcing function.

The method of constructing the models is described in Paper III. Two improvements were made. First, the brightness of the disk caused by the linear density wave was expressed in intensity rather than magnitudes since the density wave should vary the *intensity* sinusoidally around a circle centered on the center of M81. The amplitude of the linear wave nevertheless is still quoted in magnitudes. The second change involves determining the radial star formation rate. Each of the 10 models has an attached star formation rate differing from another model by a constant factor independent of distance from the center. So the procedure used here involved finding a relative radial star formation rate which, when scaled by a constant factor, would allow each of the ten models to agree with the observed surface brightness in two colors. One was found such that, in 20 comparisons (10 models times 2 colors), only one is worse than 0.10 mag arcsec^{-2}. The models cover the portion of M81 from 3 kpc from the center (the inner Lindblad resonance) out to 7.48 kpc, the last place at which the surface brightness was compared. The process also assumes that the mass spectrum of the newly born spiral arm stars does not vary with distance from the center, that all of the cluster's stars begin shining simultaneously, that all are visible, and that the reddening is the same for all spiral arm stars. Figure 6 shows the relative star formation rate.

The relative star formation rate has a rather strange looking form; however, it roughly corresponds to the plot of the ratio of the surface density of H II regions to the surface density of H I as shown in Figure 6.8 of Visser (1978). Both curves peak at about 5 kpc and fall to very low values by 8 kpc. Figure 6 shows a narrow peak at 3 kpc which Visser's figure does not show. Neither the star formation rate shown in Figure 6 nor the star formation rate (H II/H I) as shown by Visser agrees at all well with the relative shock strength as a function of R. The shock strength rises smoothly from 3 kpc to 8 kpc, after which it drops. The simple conclusion may just be that the relative shock strength, alone, does not measure the star formation rate.

Figure 7 shows the spiral arm colors $(U-B)_A$ and $(B-V)_A$ for each of the 10 models and defined exactly as in Schweizer (1976). Each set of models using the same cluster model is connected by a straight line labeled with the cluster model, A, B, or C. Each model value of the spiral arm colors is plotted with the heavy dot and labeled with the linear density wave amplitude. The model value is just the mean of the individual colors

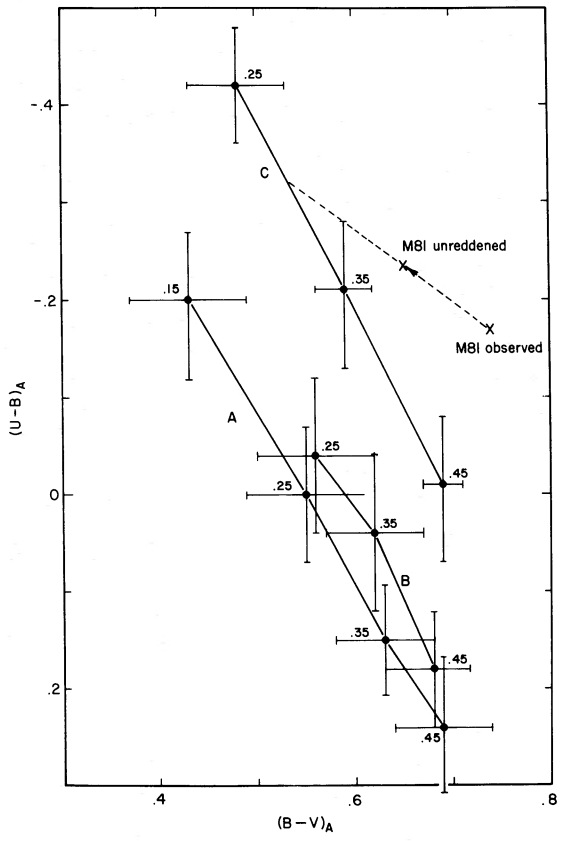

FIG. 7.—The colors of the spiral arms in models of M81, in each of which the computed surface brightness agrees with the observed values. Each heavy dot is marked by the initial mass spectrum used (A,B,C) and the linear-density-wave amplitude in the old disk. Schweizer's observed value for the arm colors of M81 is marked, as is a value unreddened by $E(B-V)=0.09$ mag. Each model covers seven different radii at which Schweizer observed M81 between $3 \leq R \leq 7.48$ kpc.

computed at the seven radii $R=3.86$ kpc through 7.48 kpc. The total star formation rate for the region $3 \leq R \leq 7.48$ kpc for each model is shown in Table 2. Each model point is also shown with error bars. The distance from the model point to the end of the error bar is the root mean square scatter about a straight line fit to each color index as a function of R. Figure 8 shows the color index for the arms at each of the seven radii and the best-fitting straight line for the model with mass function C and density wave amplitude 0.25 mag. Note that the values plotted on Figure 7 are marked by a cross. The size of the error bars in Figure 7 could be reduced by fitting more complex functions to the run of computed colors in Figure 8, but no justification for such a procedure could be found. Finally, Figure 7 includes Schweizer's measured value for the spiral arm colors in M81, and Schweizer's value de-reddened by $E(B-V)=0.09$ mag, which was estimated by using the formulae in de Vaucouleurs, de Vaucouleurs, and Corwin (1976) to obtain face-on, reddening-free colors. But comparison of the model and observations has problems: for example, the points in Figure 7 have rather large uncertainties, the precise region which Schweizer (1976) used in defining his observed value is not clear, the transformation from Schweizer's U, B_3, O photometric system to $(B-V)$ color is based on an empirical relation fit to galaxy colors and may be extra uncertain, and the measures of $(U-B_3)$ and (B_3-O) colors used to obtain $(U-B)$ and $(B-V)$ colors have uncertainties of $\sigma \approx 0.1-0.2$ mag. However, Schweizer's measured arm colors as unreddened seem most consistent with mass spectrum C and a linear density wave amplitude of 0.25–0.35 mag. In spite of the uncertainties, there is independent evidence that this choice is correct. Schweizer separately measured the amplitude of the linear density wave in the old, red disk for M81 and obtained an average value of 0.23 mag. This suggests that cluster model C is correct since the observed value for M81 in Figure 7 would have to be moved down and to the left by nearly 0.3 mag to be consistent with either cluster model A or B *and* a linear density wave amplitude of ~ 0.25 mag.

The model values of color indices plotted on Figure 7 are averages of the seven computed values. Integrated colors of the model arms have also been computed. In each case they are about 0.03 mag redder in both $(U-B)_A$ and $(B-V)_A$ than the points plotted. It has been suggested to us that Schweizer has computed observed, integrated color indices and that these model integrated colors are even closer to Schweizer's observed value than the values plotted in Figure 7. Since the arms are brighter and redder at small radii than they are at larger radii, the contribution of the arms inside $R=3$ kpc, which are not included in the model, should be removed from Schweizer's observed value. We do not know how to do this, but such a procedure should further improve the resemblance between cluster model C and the observations.

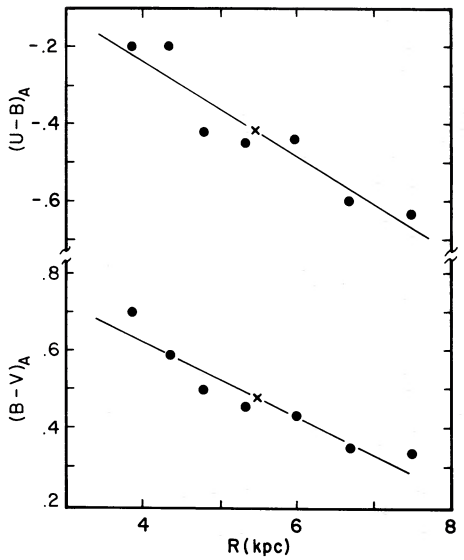

FIG. 8.—Details of the radial arm-color dependence for the model using mass spectrum C and density wave amplitude 0.25 mag. The error bars in Fig. 7 show the scatter of the seven computed colors about the best-fitting straight line. The average values, plotted on Fig. 7, are marked by the cross.

TABLE 2

STELLAR BIRTHRATE ($M_\odot$ yr^{-1}) ($3 \leq R \leq 7.48$ kpc)

DISK DENSITY-WAVE AMPLITUDE (mag)	CLUSTER MODELS A	B	C
0.15	0.19	...	...
0.25	0.16	0.13	0.09
0.35	0.13	0.11	0.08
0.45	0.11	0.09	0.05

Cluster model C (as shown in Paper III) includes an extremely large relative number of high-mass stars with 83% by number, and 99^+% by mass, more massive than 10 $M_\odot$. Miller and Scalo (1979) find that in the Orion OB1 association, the initial mass function (IMF) slope for $M \geq 2$ $M_\odot$ agrees well with the field star IMF. If Orion OB1 is typical of the mass spectrum of the spiral arm process, then the low mass stars in the arms often must be hidden in dust or not yet on the main sequence during the lifetimes of massive stars.

Schweizer (1976), as shown in his Table 5, finds that B9 stars reproduce the $U-B$ color of the spiral arms in M81, yet we claim that O stars are required. This difference is due to the fact that the linear density wave in the old disk enhances the brightness of the disk under the spiral arms of young stars. This enhancement is not removed by the method Schweizer used to define the

spiral arms, as he realized. The combination of spiral arms of O stars plus the enhanced brightness of the old, red disk makes the composite spectral type later than the spectral type of the young stars. Therefore Schweizer's result and ours are not in conflict.

Finally, we ask if this model produces something which looks like M81. Figure 9 [Plate 15] shows a face-on view of our model of M81. The galaxy is divided into cells 260 pc on a side and those cells through which the potential minimum runs are set to black. In the remaining cells, the surface brightness in the *B*-filter is computed using cluster model C, linear disk density wave amplitude of 0.35 mag for which the spiral-arm star formation rate is 0.08 $M_\odot$ yr^{-1} in the portion of the galaxy covered by our model, $3 \leq R \leq 7.48$ kpc. The arms have an underlying exponential stellar disk which extends into the center. The surface brightness key is marked. The darker the square, the brighter it is. Surface brightness in mag arcsec^{-2} is equal to this unit plus 36.57, and the major axis runs vertically through the center. Figure 10 [Plate 16] shows this same picture tilted at 59° about the major axis compared to Visser's (1978) Figure 6.5. Visser's figure shows a 200 inch (5 m) photograph of M81 with the potential minimum (*dashed line*) and the TASS wave (*full line*). The dashed line in Visser's photograph should be compared to the black spiral trace in Figures 9 and 10 and to the spiral shown in Figures 2, 3, and 4.

We compare the model's surface brightness to the photograph of M81 starting at the ends of the spiral trace and working in. First the ends of the model spiral arms in Figures 9 and 10 are beyond the edge of the model at $R = 7.5$ kpc. The dynamical model is defined at that place, but the surface brightness is not properly set there, so the brightness at the bright ends of the arms should be ignored. Now note that the brightest portion of the model spiral arms runs along inside of the potential minimum and then crosses it at about the place where the potential minimum crosses the major axis. This can also be seen in M81, especially along the arm north and west of the center. Also note how the region between the arms gets progressively brighter as one moves inward. In the tilted model in Figure 10, the surface brightness gradient on the outside edge of the potential minimum just west and south of the center is expected to be, and is seen to be, quite steep. The same is true at the same place on the other side of the center. In the region south and east of the center, the model seems even to reproduce the details of the patch of bright stars which swing outside the potential minimum. At the inner end of the potential minimum south and east of the center there is evidence in the model and in the photograph for a group of very bright stars which group curves underneath the center of M81. There is very little evidence for a similar pattern north of the center in the photograph. The model's arms do not appear to be as wide as the galaxy's in the outer parts. The outer portions of the model arms do not cross the potential minimum, but arm light is seen beyond the dashed curve in the photograph in Figure 10. Although the model is too simple, it seems to produce a galaxy which in many details resembles M81. The addition of a small amount of stochastic star formation (Seiden and Gerola 1979) plus explicit account of the dust patchiness might improve the appearance and width of the arms and improve the resemblance.

IV. SUMMARY

The ballistic particle model which connects spiral structure, molecular clouds, and star formation has been fitted to M81. The model assumes that molecular clouds form in the TASS wave at the postshock velocity and that stars form in these clouds 25 million years after the clouds' birth in the spiral shock wave. The clouds and the stars which form from them are assumed to move along ballistic orbits. Visser (1978) has fitted the shock wave to observations of the H I gas in M81 and his work entirely fixes the initial conditions for the dynamical model for molecular cloud and star orbits.

The dynamical model allowed us to predict where CO emission lines from molecular clouds should be seen in M81 and to note that the one detection of CO is consistent with our prediction. We also compared our predicted H II region distribution against that observed and found good general agreement for the eastern arm. We also predicted velocity differences between H II regions and CO clouds along the major and minor axes.

We examined the predicted *UBV* surface brightness. It depends on the dynamical model, the zero-age mass spectrum for the stars, the linear density-wave amplitude in the disk, and the star formation rate. Theoretically there is only one combination of the latter three free parameters which can reproduce the observed surface brightness and spiral arm colors in M81. Because of the uncertainty of the computed and measured colors, the set of values of mass spectrum, disk density wave amplitude, and star formation rate is not uniquely defined but seems to require a mass spectrum consisting mainly of O and B stars for the spiral-arm star formation process, a density-wave amplitude of 0.25–0.35 mag in agreement with Schweizer's measured average value of 0.23 mag, and a star formation rate for the region $3 \leq R \leq 7.5$ kpc of 0.08 $M_\odot$ yr^{-1}. The star formation rate is surprisingly small owing to the fact that the freshly formed stars are very luminous per unit mass, and presumably also to the rather early Hubble type for M81. The extreme spiral arm mass spectrum is also very interesting. It is forced on us in order to reproduce the arm colors. The details of the predictions of luminosity and color for that mass spectrum, reported in Paper III, use our model C in which nearly all of the mass is in stars more massive than 10 $M_\odot$. It is possible that the

low-mass stars are hidden from view or that they form later so that the actual mass spectrum and the one which one sees near the arms are different.

There is, perhaps, some doubt that the spiral-arm star formation process extends to low-mass stars which are hidden. If we use a typical mass spectrum for the process,

$$n(M)dM = KM^{-P}dM$$

with $P=2.5$ from 100 $M_\odot$ through 1 $M_\odot$ and $P=1.0$ from 1 $M_\odot$ to 0.1 $M_\odot$, then, if the mass birthrate is 0.08 $M_\odot$ yr^{-1} for stars of mass not less than 15 $M_\odot$, the whole birthrate down to 0.1 $M_\odot$ would be 14 $M_\odot$ yr^{-1}, which seems prohibitively large. Therefore, either this paper is wrong or the spiral arm star formation process does not make very many low-mass stars. This may suggest that star formation in spiral galaxies must be described by at least two different initial mass functions and that the IMF which we regard as typical is appropriate only to the interarm regions.

The work reported here is preliminary, but an attack on M81 seems capable of answering important questions. First, measured surface brightness in the *UBVR* bands of the quality and in the detail reported by Schweizer (1976) is needed. Work in these conventional bands would allow quantitative comparison of computed tracks with observed colors since bolometric corrections are available for the *UBV* system. Second, the model O star tracks need to include mass loss; however, it should be pointed out that, since such tracks tend to make the stars redder, this is unlikely to change our conclusions regarding the mass spectrum of the spiral arm stars, only to reinforce them. Third, in this work, the absolute star formation rate ($M_\odot$ yr^{-1}) depends critically on the stellar upper-limit mass and on the properties of the most massive O stars, so such tracks also need to be computed. Fourth, as they become possible in the near future, CO observations in M81 are crucial in deciding whether our model is correct. Fifth, radial-velocity measurements of the H II regions are also needed, especially near the eastern arm, since our model also predicts them. Such measurements are currently possible but difficult.

Visser (1978) has clearly shown that the density wave is present in the H I gas in M81. This work applies the ballistic particle model which connects the H I gas with the dense molecular gas and the spiral arm stars. In the case of M81, we seem to have a chance for a definitive test of the effect of the density wave and a chance to find out what kind of stars the spiral arms make.

We would like to thank Margaret Knox and the staff of the University of Texas Computation Center's Advanced Graphic Laboratory for their kind and willing help in producing the model pictures of M81. This work was also supported in part by NSF grant AST 79-20966.

REFERENCES

Bash, F. N. 1979, *Ap. J.*, **233**, 524 (Paper III).
Bash, F. N., Green, E., and Peters, W. L. 1977, *Ap. J.*, **217**, 464 (Paper II).
Bash, F. N., and Peters, W. L. 1976, *Ap. J.*, **205**, 786 (Paper I).
Combes, F., Encrenaz, P. J., Lucas, R., and Weliachew, L. 1977, *Astr. Ap.*, **55**, 311.
Connolly, L. P., Mantarakis, P. Z., and Thompson, L. A. 1972, *Pub. A.S.P.*, **84**, 61 (CMT).
de Vaucouleurs, G., de Vaucouleurs, A., and Corwin, H. G., Jr. 1976, *Second Reference Catalogue of Bright Galaxies* (Austin: University of Texas Press).
Ford, H. C., and Jenner, D. C. 1978, *Bull. AAS*, **10**, 665.
Mezger, P. G. 1970, in *IAU Symposium 38, The Spiral Structure of Our Galaxy*, ed. W. Becker and G. Contopoulos (Dordrecht: Reidel), p. 107.
Miller, G. E., and Scalo, J. M. 1979, *Ap. J. Suppl.*, **41**, 513.
Roberts, W. W., Roberts, M. S., and Shu, F. H. 1975, *Ap. J.*, **196**, 381.
Rots, A. H. 1975, *Astr. Ap.*, **45**, 43.
Rots, A. H., and Shane, W. W. 1975, *Astr. Ap.*, **45**, 25.
Schweizer, F. 1976, *Ap. J. Suppl.*, **31**, 313.
Seiden, P. E., and Gerola, H. 1979, *Ap. J.*, **233**, 56.
Stark, A. 1979, doctoral thesis, Princeton University.
van den Bergh, S. 1960, *Ap. J.*, **131**, 558.
Visser, H. C. D. 1978, doctoral thesis, University of Groningen.

FRANK N. BASH: Astronomy Department, University of Texas, Austin, TX 78712

HERMAN C. D. VISSER: Berkeley Astronomy Department, University of California, Berkeley, CA 94720

PLATE 15

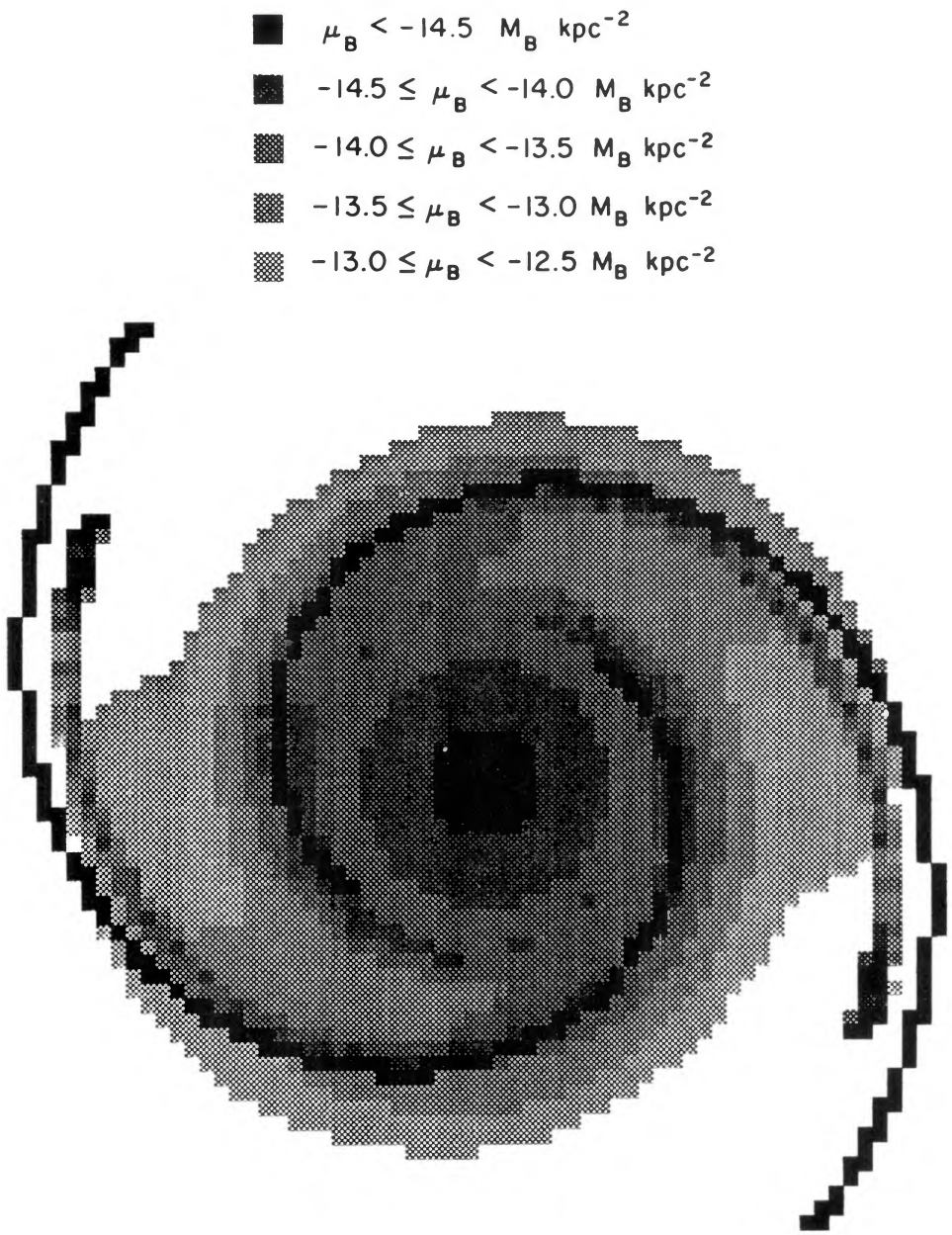

FIG. 9.—A face-on view of a model of the surface brightness of M81 in the *B*-filter. This model uses mass spectrum C and linear density wave amplitude 0.35 mag. The galaxy is divided into cells 260 pc on a side. The cells through which the potential minimum runs are set black. The remaining cells show the computed surface brightness where the darker the cell, the brighter it is computed to be.

BASH AND VISSER (*see* page 497)

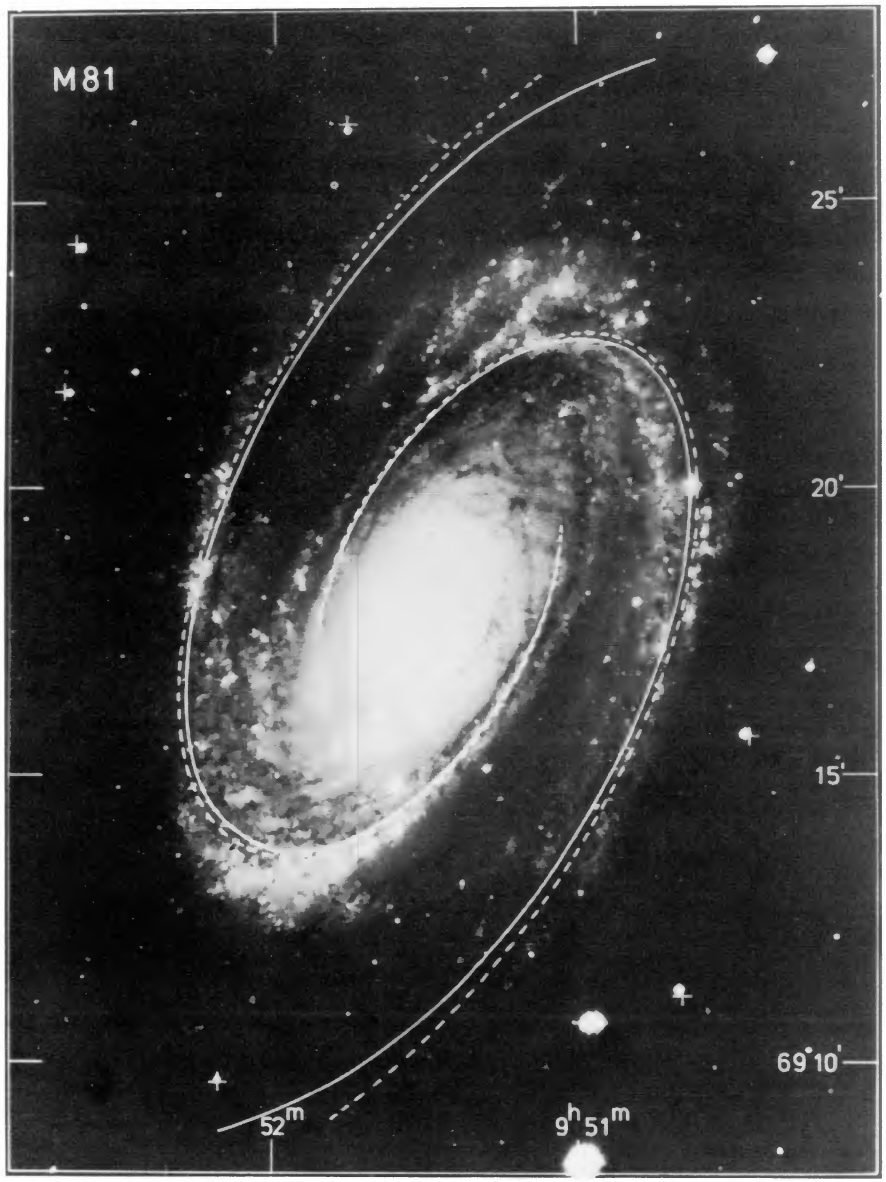

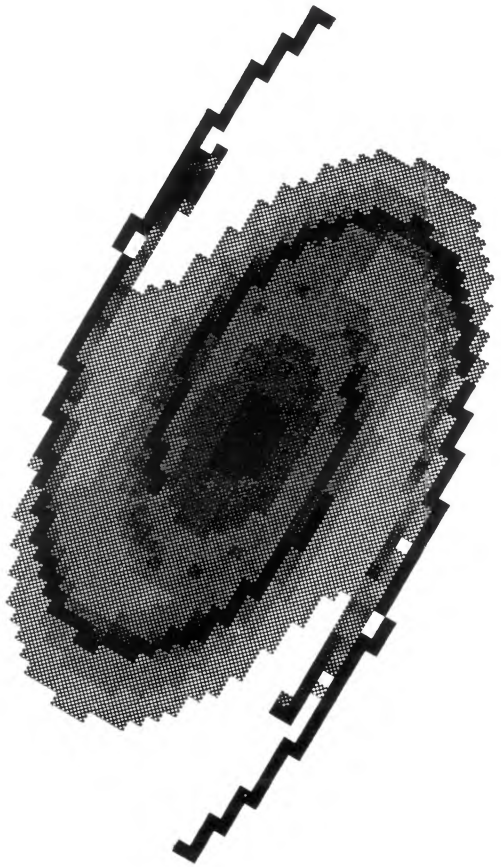

FIG. 10.—The model in Fig. 9 inclined by 59° compared to Visser's (1978) Fig. 6.5. In the photograph, the potential minimum is shown by the dashed line and the TASS wave by the full line. (Photograph courtesy of the Hale Observatories.)

BASH AND VISSER (*see* page 497)